Estimation of the lower ionosphere ionization caused by X-class solar flares, based on VLF observations

I.A. Ryakhovsky[1], Y.V. Poklad[1], B.G. Gavrilov[1], S.Z. Bekker[1]

[1]Sadovsky Institute of Geospheres Dynamics, Russian Academy of Sciences, Moscow, Russia

Key Points:

- The dynamics of the lower ionosphere during solar flares were estimated from parameters of VLF signal on the two-frequency path
- The GOES data made it possible to estimate the source brightness temperature and the radiation dynamics in a wide X-ray wavelength range
- The ionization and recombination rates and spectral ranges of radiation with greatest influence on the ionization processes were determined

Corresponding author: Ilya Ryakhovsky, ryakhovskiy88@yandex.ru

Abstract

We present the results of the analysis of the measurements data of amplitudes and phases of signals from GQD (19.58 kHz) and GBZ (22.1 kHz) VLF transmitters in the geophysical observatory of IDG RAS "Mikhnevo" (GO MIK) to assess the impact of solar flares of different classes that occurred in June 2014 on the height profile of the electronic concentration Ne in the lower ionosphere. The use of two-channel data from the GOES satellite (0.05-0.4 nm and 0.1-0.8 nm) allowed us to estimate the fluxes of X-rays in harder spectral ranges. The analysis of the dynamics of the Ne height profile and X-ray fluxes in different wavelength ranges allowed us to estimate the ionization and recombination rates and determine the spectral ranges of radiation that have the greatest influence on the dynamics of the electron concentration at considered heights.

Plain Language Summary

The state and dynamics of the lower ionosphere (D region), which change strongly during solar flares, largely determine the conditions for VLF radio wave propagation. At the same time, analysis of these radio wave parameters, together with data on solar flare parameters obtained from satellite measurements, makes it possible to study the changes taking place in the ionosphere. The main source of flare data is the GOES satellite, which measures the X-ray flux at two frequency bands only: 0.05-0.4 nm and 0.1-0.8 nm. How radiation at other wavelengths affects the ionosphere remains unknown. We were able to determine the brightness temperature of the source (the selected solar flare) from the GOES data and calculate the dynamics of the radiation flux at other wavelengths. Our studies resulted in data on spectral ranges of radiation having the greatest influence on the processes of ionization of the lower ionosphere, which, in turn, allowed us to estimate the rates of ionization and recombination of the lower ionosphere during solar flares.

1 Introduction

Electromagnetic radiation caused by solar flares of various classes has a significant impact on the height profile of the electron concentration of the entire ionosphere. The D-region is the most difficult for experimental and theoretical study (Bekker et al., 2021, 2022). During solar flares flux of X-ray radiation of the Sun penetrates into D-region and increases electron concentration by several times due to additional ionization (Mitra, 1974; Kumar & Kumar, 2018). The results of numerous studies have shown that changes in the electron concentration in the lower ionosphere affect the parameters of VLF electromagnetic signals propagating in the Earth-ionosphere waveguide (Thomson, 2010; Thomson et al., 2011). Establishing the mechanisms of this influence makes the study of VLF electromagnetic radiation parameters an effective tool for assessing the state and dynamics of the lower ionosphere under calm and perturbed conditions (Gavrilov et al., 2019).

In Gavrilov et al. (2019) a method of reconstruction of ionospheric parameters using the two-parameter Wait-Ferguson model (Ferguson, 1995) was tested using data of radio signal parameters on a two-frequency mid-latitude VLF path formed by GQD and GBZ transmitters in United Kingdom and VLF receiver in GO MIK (54°57‘ N, 37°46‘ E). Within the framework of this model, the high-altitude profile of the electron concentration is given by the equation:

$$Ne(h) = 1.43 \cdot 10^7 exp(\beta - 0.15)(h - h')exp(-0.15 \cdot h') \quad (1)$$

where h' (km) is the effective reflection height of the radio signal and $\beta(km^{-1})$ is the rate of increase in electron concentration (cm^{-3}) with height.

The use of a two-frequency path made it possible to assess not only the dynamics of the ionosphere during a flare, but also its state before the flare.

The main processes influencing the state and dynamics of the ionosphere (without taking into account the processes of diffusion and plasma drift) are the ionization of neutral components and recombination of charged particles. This paper presents the results of the analysis of the ionization and recombination processes of the lower ionosphere during the C, M, and X-class solar flares that occurred on June 10 and 11, 2014.

2 Statement and Results of the Experiment

Since 2014, GO MIK has been continuously monitoring the amplitude and phase characteristics of signals from VLF radio transmitters located around the world (Figure 1.) (Ryakhovskii et al., 2021). The signals are recorded by a Metronix-ADU07 high-frequency measuring complex on horizontal magnetic antennas oriented in the North-South and East-West directions. The obtained waveforms of magnetic field variations with a sampling frequency of 132 kHz allow us to study the time course of the amplitude and relative phase of the signals of the VLF transmitters with a frequency resolution of 1 Hz.

Table 1 shows the temporal characteristics of solar flares (start, time of maximum of radiation flux, and end of flare) recorded in the GO MIK in June 2014, for which the processes occurring in the lower ionosphere were estimated from the data of variations in the amplitude and phase characteristics of VLF signals.

The use of data from the two-frequency GQD/GBZ - GO MIK paths and the Wait-Ferguson model (Gavrilov et al., 2020) allowed us to estimate the electron concentration (Ne) dynamics at different heights. The results of calculations of signal amplitude and phase variations on the GQD/GBZ - GO MIK path are shown in Figure 2, which also shows X-ray emission fluxes at wavelengths of 0.05-0.4 nm and 0.1-0.8 nm recorded by the GOES satellite during the X2.2 flare on 10.06.2014. It is characterized by a steep leading edge and short duration. For the range 0.1-0.8 nm, the flux rise time from 0.1 level to the maximum was 2 min, and the total duration of the flare at 0.1 level from the maximum was 7.5 min. For the 0.05-0.4 nm range, these values were 1.5 min and 5.5 min, respectively. The same figure shows the results of calculations using the Wait-Ferguson model of the dynamics of Ne values for heights of 52, 56, 60, and 64 km.

Since the altitude profile described by equation (1) is exponential, the question arises about the limits of applicability of this equation for estimating the electron concentration. The Wait-Ferguson model is radiophysical and is based on the analysis of data on the propagation of VHF radio signals. That is, the model, correctly describes the range of electron concentration, which affects the reflection parameters of radio waves of this frequency range. We used the concentration range from 10 cm^{-3} to 3500 cm^{-3}. Its upper boundary is marked in Figure 2d with a horizontal dotted line. Smaller concentration have no significant effect on the parameters of the VLF electromagnetic wave, and at higher values of electron concentration the VLF radio waves experience a complete reflection.

The dynamics of Ne in the D region of the ionosphere can be described with a simple scheme of the ionization-recombination cycle presented on Figure 3.

Within this model, the ionization rate is determined by the radiation flux I with the coefficient K_i. The coefficients K_1 and K_2 describe the processes of electrons attachment to the neutrals and recombination of electrons on the positive ions, respectively. The coefficient K_n describes the process of recombination ion-ion recombination.

These processes can generally be described by a system of equations:

$$\begin{cases} \frac{dN^-}{dt} = K_1 N_e - K_n N^- (N_e + N^-) \\ \frac{dN_e}{dt} = K_i I - K_1 N_e - K_2 N_e (N_e + N^-) \end{cases} \quad (2)$$

where N_e and N^- are concentrations of electrons and negative ions respectively, concentration of positive ions was calculated as $N^+ = N_e + N^-$.

Assuming that the source of radiation during an X-ray flare is a black-body (Levine et al., 2019; Gavrilov et al., 2022), its spectral density obeys Planck's law:

$$I(\lambda, T) = \frac{2\pi\hbar c^2}{\lambda^5} \frac{1}{exp(\frac{\hbar c}{\lambda k T}) - 1} \tag{3}$$

where h is Planck constant, c is the speed of light, k is Boltzmann constant, λ is the wavelength, T is the brightness temperature of the black body.

Then the data of radiation flux measurements by the GOES satellite allow us to estimate the brightness temperature T of the source, i.e., the temperature for which the condition is satisfied:

$$\frac{\int_{0.1}^{0.8} I(\lambda, T) d\lambda}{\int_{0.05}^{0.4} I(\lambda, T) d\lambda} = \frac{F_2}{F_1} \tag{4}$$

where F_1 is the radiation flux in the range 0.05-0.4 nm, and F_2 in the range 0.1-0.8 nm.

Using the brightness temperature calculated from GOES data makes it possible to estimate radiation fluxes in other spectral ranges.

Figure 4 shows experimental data on X-ray fluxes detected by the GOES satellite during the X2.2 flare on 10.06.2014 at 0.05-0.4 nm and 0.1-0.8 nm, as well as calculated fluxes at wavelengths 0.01-0.3, 0.01-0.26 and 0.01-0.22 nm.

Note that as the upper limit of the range decreases, the flux decreases, and the steepness of the leading and trailing fronts increases.

Figure 2b,c shows that 50 min after the onset of the flare, the amplitude and phase of the signals have not returned to the pre-flare state, i.e., the characteristic times of recombination processes are significantly longer than the rise time of the front. In this case, the system of equations (2) can be reduced to the form:

$$\frac{dN_e(h,t)}{dt} = K_i(h, \lambda) \cdot I(\lambda, t) \tag{5}$$

By integrating (5) over time, we obtain:

$$dN_e(h,t) = K_i(h, \lambda) \cdot E(\lambda, t) \tag{6}$$

where E is the radiation energy. It follows from formula (6) that at the leading edge of a short flare, the concentration of electrons must be proportional to the energy of the radiation.

Figure 5 shows the dependencies of electron concentration on the energy of X-ray radiation at heights of 52, 56, 60, and 64 km calculated using the Wait-Ferguson model (1) for different spectral ranges. When calculating the energy of radiation, the value of the zenith angle of the Sun was taken into account.

Figure 5 shows that the dependence of the electron concentration on the radiation energy at the flare front is close to linear, which corresponds to model (6).

Further calculations were performed for spectral ranges, where the lower bound was 0.01 nm, and the upper bound varied from 0.18 nm to 0.32 nm. To calculate the coefficient at the considered heights, Ne values (calculated by the Wait-Ferguson model) were taken for the time period from the flare onset to the moment when 95% of the emission maximum in the spectral range of 0.05-0.4 nm was reached (the red rectangle in Figure 2).

The K_n coefficient describing the process of ion-ion recombination was estimated using the ratio presented in (Sentman et al., 2008):

$$K_n = 2 \cdot 10^{-7} \Big(\frac{300}{T} \Big)^{0.5} \tag{7}$$

The temperature distribution by altitude was taken from the model NRLMSISE-00. The values of temperature and K_n coefficients for the considered heights are presented in Table 2.

To estimate the coefficients K_1 and K_2 (equation 2), the Ne values at the flare back front were taken for each height, starting from the moment when the radiation flux in the spectral range of 0.05-0.4 nm became less than 30% of the maximum value. This time range is marked with a green rectangle in Figure 2.

In the last step, we corrected the K_i, K_1, and K_2 values so that the dependence of the electron concentration on time calculated by equation (2) corresponded best to the time course of the electron concentration calculated by the Wait-Ferguson model (1) for each of the heights. A comparison of the results of the calculation of the Ne dynamics for different spectral ranges with the Ne data calculated by the Wait-Ferguson model is presented in Figure 6.

Figure 6 shows that for different spectral ranges it is possible to select the values of K_i, K_1, and K_2 so that the curve qualitatively describes the Ne dynamics calculated using the Wait-Ferguson model at any of the heights under consideration. To resolve the uncertainty in the choice of K_i, K_1, and K_2 coefficients and to estimate the contribution of different spectral bands at each of the heights in question, we additionally used the X 1.5 flare that occurred on the same day at 12:50 UT. Figure 7 shows the concentration calculations at different heights for both flares. Thus, the use of experimental data on the variation of the amplitude-phase characteristics of VLF-band signals during two X-class solar flares allowed us to estimate:

- The ionization and recombination rate coefficients that most effectively describe the dynamics of Ne at considered heights, and spectral ranges of radiation that have the greatest influence on ionization processes for the heights in question;

- Figure 7 shows that at each altitude the spectral range of X-ray radiation that has the greatest influence on the dynamics of Ne can be distinguished.

The results of these assessments are presented in Table 3. They allowed us to estimate the Ne dynamics during flares of M and C classes that occurred on June 10 and 11, 2014 (Table 1). High-altitude Ne profiles of the lower ionosphere obtained for these flares were further used to calculate possible amplitude-phase characteristics of signals measured in GO MIK from GQD transmitter and compared with the results of measurements (Figure 8). The qualitative coincidence of the calculated values with the results of experimental measurements testifies to the correctness of the proposed methodology.

3 Conclusion

Many works have been devoted to the study of the impact of X-ray radiation from solar flares on the ionosphere and, in particular, on its lower layers. Nevertheless, the question of the wavelength range that has the greatest influence on the electron concentration profile in the lower ionosphere has not been sufficiently investigated. This is due to the limited amount of data on the radiation spectrum of solar flares. The present work attempts to elucidate this question. To this end, the radiation flux in wavelength ranges beyond the limits of GOES satellite measurements was calculated for a number of known flares.

In this work we use the methodology of restoration of ionospheric parameters within the framework of the two-parameter Wait-Ferguson model from data of radio signal measurements on a two-frequency mid-latitude VLF path, formed by GQD and GBZ transmitters in United Kingdom and VLF receivers in GO MIK. Note that the Waite-Ferguson model is radiophysical, and it correctly describes only the range of electron concentration that affects the parameters of VLF radio wave propagation.

This paper presents the results of an assessment of the ionization and recombination processes of the lower ionosphere during the C, M, and X-class solar flares that occurred on June 10 and 11, 2014. For convenience and to formalize the results of the study, we introduced K coefficients describing the processes of electrons attachment to the neutrals and recombination of electrons and negative ions on the positive ions.

The study of the ionization efficiency of the lower ionosphere by radiation with different wavelengths is carried out by calculating the brightness temperature of the source, assuming that the source of radiation during the flare in the X-ray range is a black-body and its spectral density obeys Plank's law. After making the necessary calculations of the electron profile of the ionosphere during the X2.2 flare (10.06.2014), the values of K coefficients were corrected so that the dependence of the electron concentration on time best suited the time course of the electron concentration calculated by the Wait-Ferguson model for each of the heights. Uncertainties in the determination of the ionization and recombination coefficients were eliminated by analyzing data from the X1.5 flare, which occurred on the same day at 12:50 UT.

The use of experimental data on the variation of the amplitude-phase characteristics of VLF band signals during two X-class solar flares allowed us to estimate the dynamics of ionization and recombination rates that most effectively describe the dynamics of Ne at considered heights and the spectral emission bands that have the greatest influence on ionization processes.

The results obtained were used to estimate the Ne dynamics during the C- and M-class flares that occurred on June 10 and 11, 2014, and allowed us to solve the inverse problem: calculate the possible amplitude-phase characteristics of the signals for the selected VLF paths. Their comparison with direct measurement results confirmed the adequacy of the methods used.

4 Open Research

The VLF data set used in the present work was collected in the Mikhnevo observatory of the Sadovsky Institute of Geospheres Dynamics of Russian Academy of Sciences (`https://idg.ras.ru/data/calendar_VLF_2014.html`). The satellite data for the radiation flux obtained by the GOES satellite are available on `https://www.ncei.noaa.gov/data/goes-space-environment-monitor/access/full/`. Data of the temperature distribution by altitude was taken from the model NRLMSISE-00 (`https://ccmc.gsfc.nasa.gov/modelweb/models/nrlmsise00.php`).

Acknowledgments

This work was supported by the Russian Science Foundation (RSF Project No. 22-77-00051).

References

Bekker, S. Z., Kozlov, S. I., & Kudryavcev, V. P. (2022). Comparison and Verification of the Different Schemes for the Ionization-Recombination Cycle of the Ionospheric D-Region. *Journal of Geophysical Research:*

Space Physics, *127*(10), e2022JA030579. Retrieved from https://agupubs.onlinelibrary.wiley.com/doi/abs/10.1029/2022JA030579 (e2022JA030579 2022JA030579) doi: https://doi.org/10.1029/2022JA030579

Bekker, S. Z., Ryakhovsky, I. A., & Korsunskaya, J. A. (2021). Modeling of the Lower Ionosphere During Solar X-Ray Flares of Different Classes. *Journal of Geophysical Research: Space Physics*, *126*(2), e2020JA028767. Retrieved from https://agupubs.onlinelibrary.wiley.com/doi/abs/10.1029/2020JA028767 (e2020JA028767 2020JA028767) doi: https://doi.org/10.1029/2020JA028767

Ferguson, J. A. (1995). Ionospheric model validation at vlf and lf. *Radio Science*, *30*(3), 775-782. Retrieved from https://agupubs.onlinelibrary.wiley.com/doi/abs/10.1029/94RS03190 doi: https://doi.org/10.1029/94RS03190

Gavrilov, B. G., Ermak, V. M., Lyakhov, A. N., Poklad, Y. V., Rybakov, V. A., & Ryakhovsky, I. A. (2020, Nov 01). Reconstruction of the parameters of the lower midlatitude ionosphere in m- and x-class solar flares. *Geomagnetism and Aeronomy*, *60*(6), 747-753. Retrieved from https://doi.org/10.1134/S0016793220060043 doi: 10.1134/S0016793220060043

Gavrilov, B. G., Ermak, V. M., Poklad, Y. V., & Ryakhovskii, I. A. (2019, Sep 01). Estimate of variations in the parameters of the midlatitude lower ionosphere caused by the solar flare of september 10, 2017. *Geomagnetism and Aeronomy*, *59*(5), 587-592. Retrieved from https://doi.org/10.1134/S0016793219050049 doi: 10.1134/S0016793219050049

Gavrilov, B. G., Poklad, Y. V., Ryakhovsky, I. A., & Ermak, V. M. (2022, Feb 01). Dependence of d-region perturbations of the midlatitude ionosphere on the spectral composition of the x-ray radiation of solar flares according to experimental data. *Geomagnetism and Aeronomy*, *62*(1), 98-103. Retrieved from https://doi.org/10.1134/S0016793222020086 doi: 10.1134/S0016793222020086

Kumar, A., & Kumar, S. (2018, Feb 12). Solar flare effects on d-region ionosphere using vlf measurements during low- and high-solar activity phases of solar cycle 24. *Earth, Planets and Space*, *70*(1), 29. Retrieved from https://doi.org/10.1186/s40623-018-0794-8 doi: 10.1186/s40623-018-0794-8

Levine, E. V., Sultan, P. J., & Teig, L. J. (2019). A parameterized model of x-ray solar flare effects on the lower ionosphere and hf propagation. *Radio Science*, *54*(2), 168-180. Retrieved from https://agupubs.onlinelibrary.wiley.com/doi/abs/10.1029/2018RS006666 doi: https://doi.org/10.1029/2018RS006666

Mitra, A. (1974). *Ionospheric effects of solar flares*. Reidel. Retrieved from https://books.google.ru/books?id=vzUpAAAAYAAJ

Ryakhovskii, I. A., Gavrilov, B. G., Poklad, Y. V., Bekker, S., & Ermak, V. (2021). The state and dynamics of the ionosphere from synchronous records of ULF/VLF and HF/VHF radio signals at geophysical observatory "Mikhnevo". *Izvestiya, Physics of the Solid Earth*, *57*, 718-730.

Sentman, D. D., Stenbaek-Nielsen, H. C., McHarg, M. G., & Morrill, J. S. (2008). Correction to "plasma chemistry of sprite streamers". *Journal of Geophysical Research*, *113*.

Thomson, N. R. (2010). Daytime tropical d region parameters from short path vlf phase and amplitude. *Journal of Geophysical Research: Space Physics*, *115*(A9). Retrieved from https://agupubs.onlinelibrary.wiley.com/doi/abs/10.1029/2010JA015355 doi: https://doi.org/10.1029/2010JA015355

Thomson, N. R., Rodger, C. J., & Clilverd, M. A. (2011). Daytime d region parameters from long-path vlf phase and amplitude. *Journal of Geophysical Research: Space Physics*, *116*(A11). Retrieved from https://agupubs.onlinelibrary.wiley.com/doi/abs/10.1029/2011JA016910 doi: https://doi.org/10.1029/2011JA016910

Table 1. List of flares of C, M and X class

Date	Class	Start	Peak time	End
2014.06.10	X2.2	11:36	11:42	11:44
2014.06.10	X1.5	12:36	12:52	13:03
2014.06.10	C3.9	08:17	08:25	08:32
2014.06.10	C5.1	09:17	09:31	09:40
2014.06.10	C5.0	10:04	10:17	10:25
2014.06.11	M3.0	08:00	08:09	08:15

Table 2. Altitude distribution of the temperature T and K_n

h, km	T,° K	K_n
52	274.8	2.1e-7
56	264	2.1e-7
60	252.2	2.2e-7
64	239.1	2.2e-7

Table 3. Altitude distribution of the ionization and recombination coefficients

h, km	$Range, nm$	$K_i, cm^{-1}s^{-1}/(W/m^2)$	K_1, s^{-1}	K_2, cm^3s^{-1}
52	0.01-0.22	$3.62 \cdot 10^4$	$6.60 \cdot 10^{-4}$	$1.49 \cdot 10^{-7}$
56	0.01-0.23	$2.74 \cdot 10^5$	$6.53 \cdot 10^{-5}$	$6.95 \cdot 10^{-6}$
60	0.01-0.24	$1.83 \cdot 10^6$	$2.58 \cdot 10^{-4}$	$2.51 \cdot 10^{-6}$
64	0.01-0.26	$4.64 \cdot 10^6$	$7.14 \cdot 10^{-4}$	$7.14 \cdot 10^{-7}$

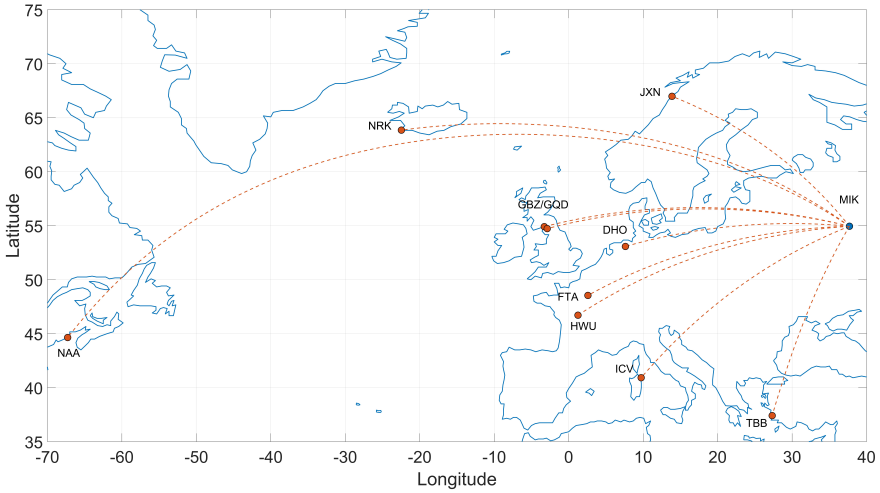

Figure 1. Location of some transmitters which signals registered in GO MIK since 2014

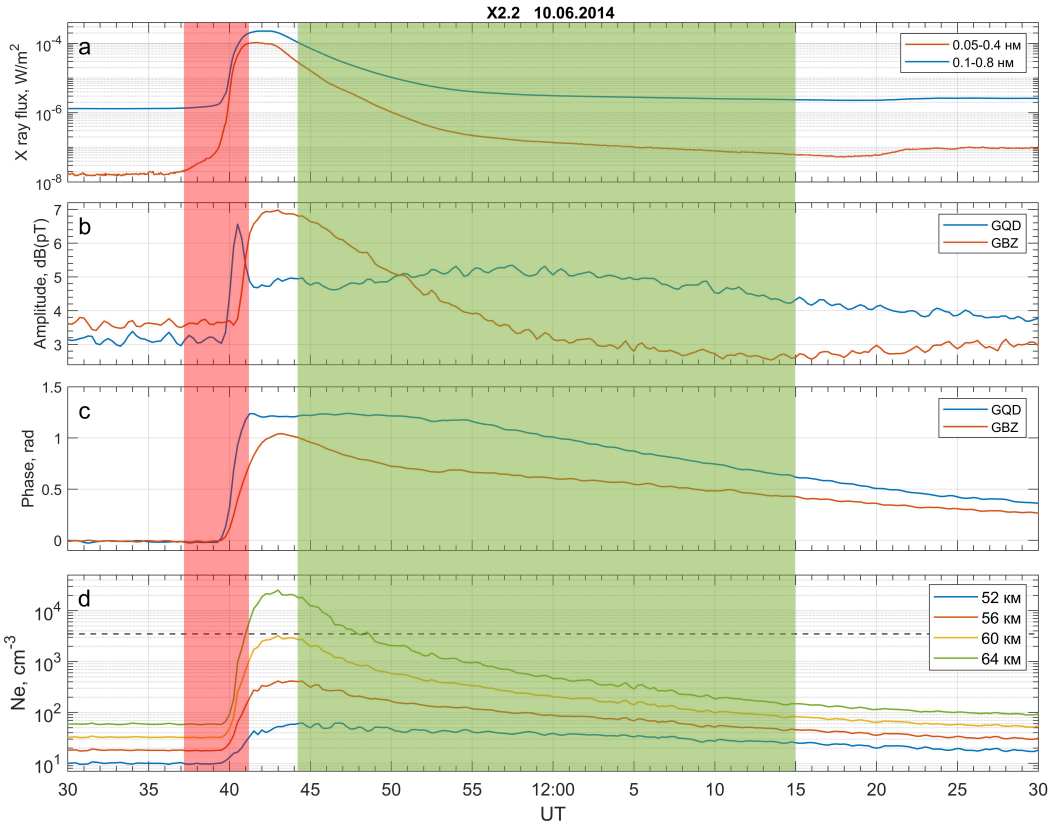

Figure 2. Dynamics of Ne during the solar flare X2.2 on 10.06.2014. (a) flux of X-rays recorded by the GOES satellite during the flare in the bands 0.05-0.4 nm (red lines) and 0.1-0.8 nm (blue lines), (b and c) signal amplitude and phase variations on the GQD/GBZ - MIK path. (d) calculations of the Ne dynamics by the Wait-Ferguson model for altitudes 52, 56, 60, and 64 km. The red rectangle shows the time interval of growth of the flare emission flux up to 95% of the maximum in the spectral range 0.05-0.4 nm. The green rectangle shows the time interval of emission flux decrease to 30% of the maximum value at the flare trailing edge for the same spectral range

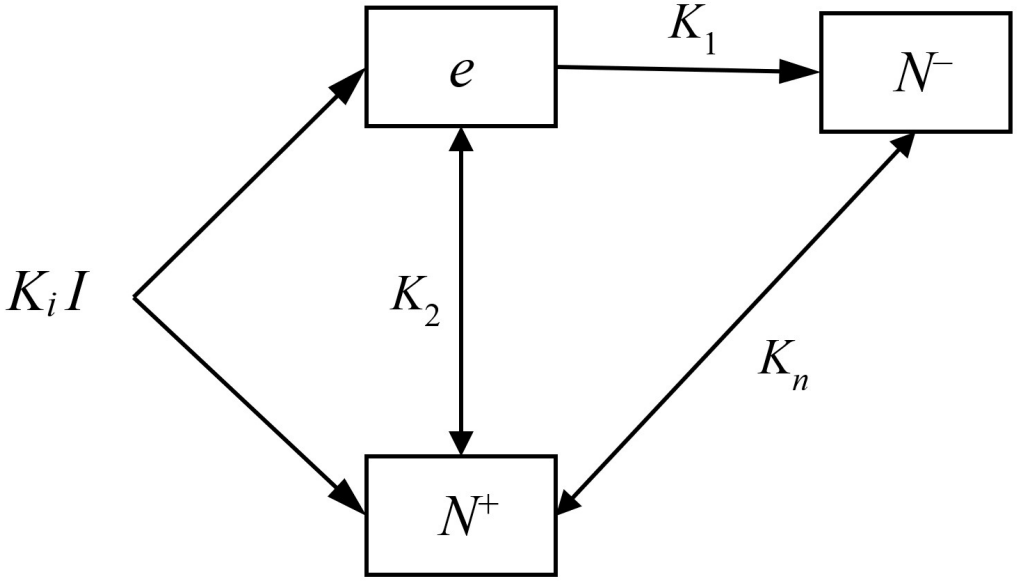

Figure 3. Simplified scheme of the ionization-recombination cycle of the lower ionosphere

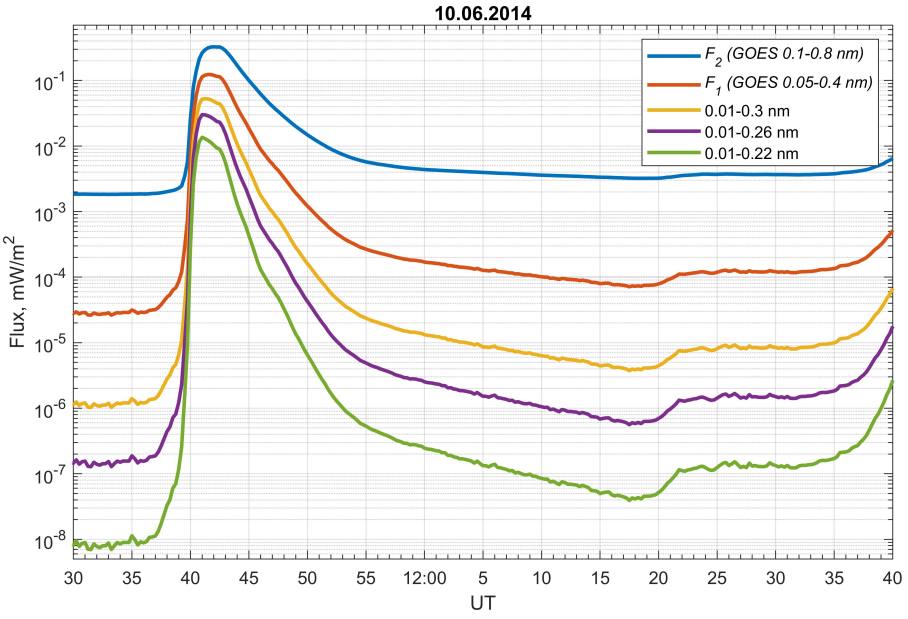

Figure 4. X-ray fluxes in different spectral ranges during the X2.2 flare on 10.06.2014

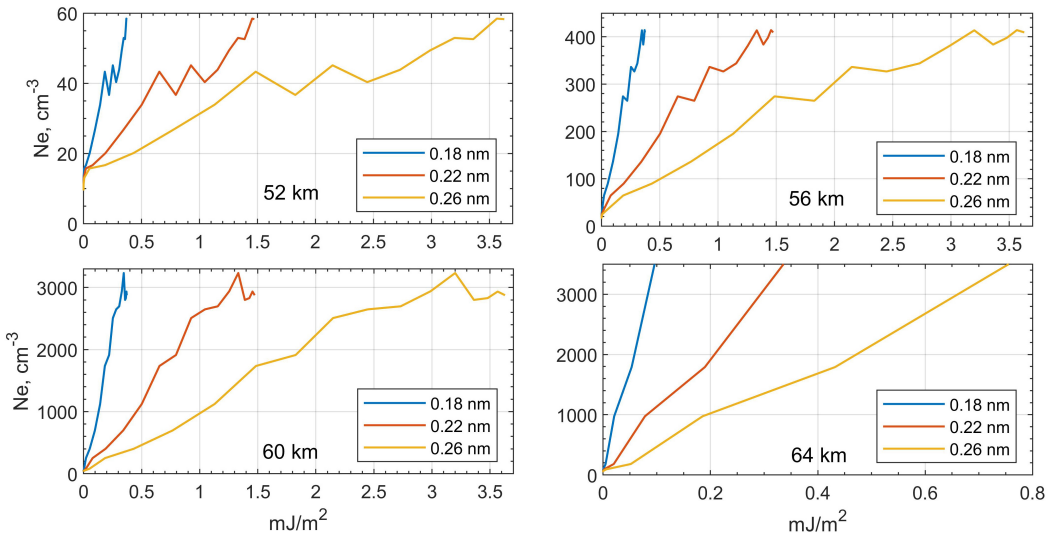

Figure 5. Dependencies of electron concentration on X-ray energy at heights of 52, 56, 60, and 64 km calculated using the Wait-Ferguson model (1)

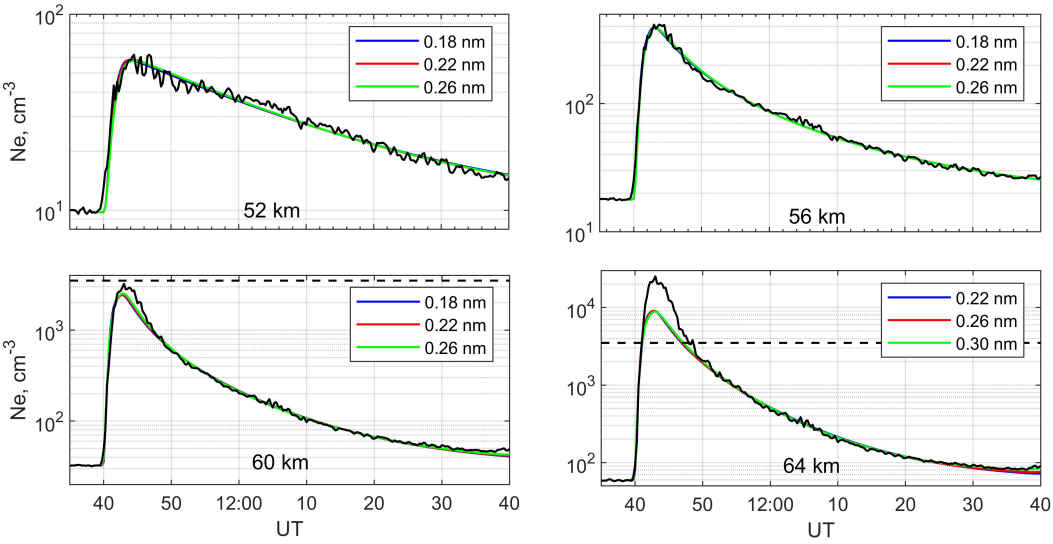

Figure 6. Dynamics of Ne during the X2.2 flare (10.06.2014), calculated according to Equation 2, for different spectral bands at heights of 52, 56, 60, and 64 km

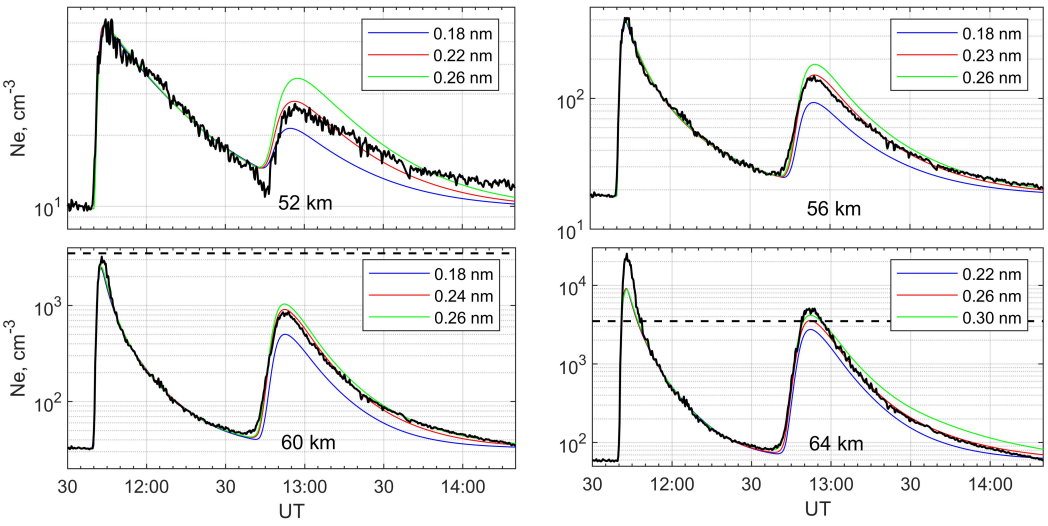

Figure 7. Dynamics of Ne during flares X2.2 and X1.5 (10.06.2014), calculated according to Equation 2 for different spectral bands at heights of 52, 56, 60, and 64 km

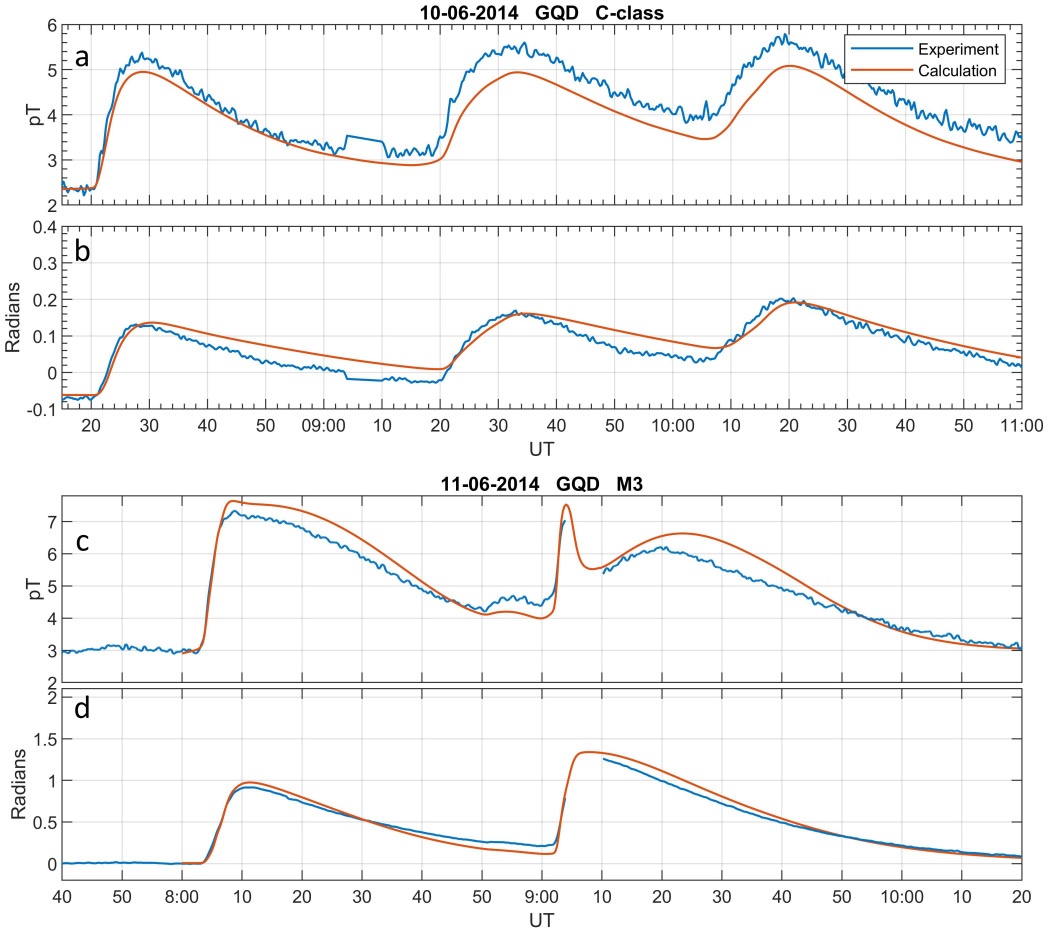

Figure 8. Experimental data (blue line) and results of calculation (red lines) of signal amplitude (a,c) and phase (b,d) variations from GQD station during C- and M-class solar flares on June 10 and 11, 2014

Figure 1.

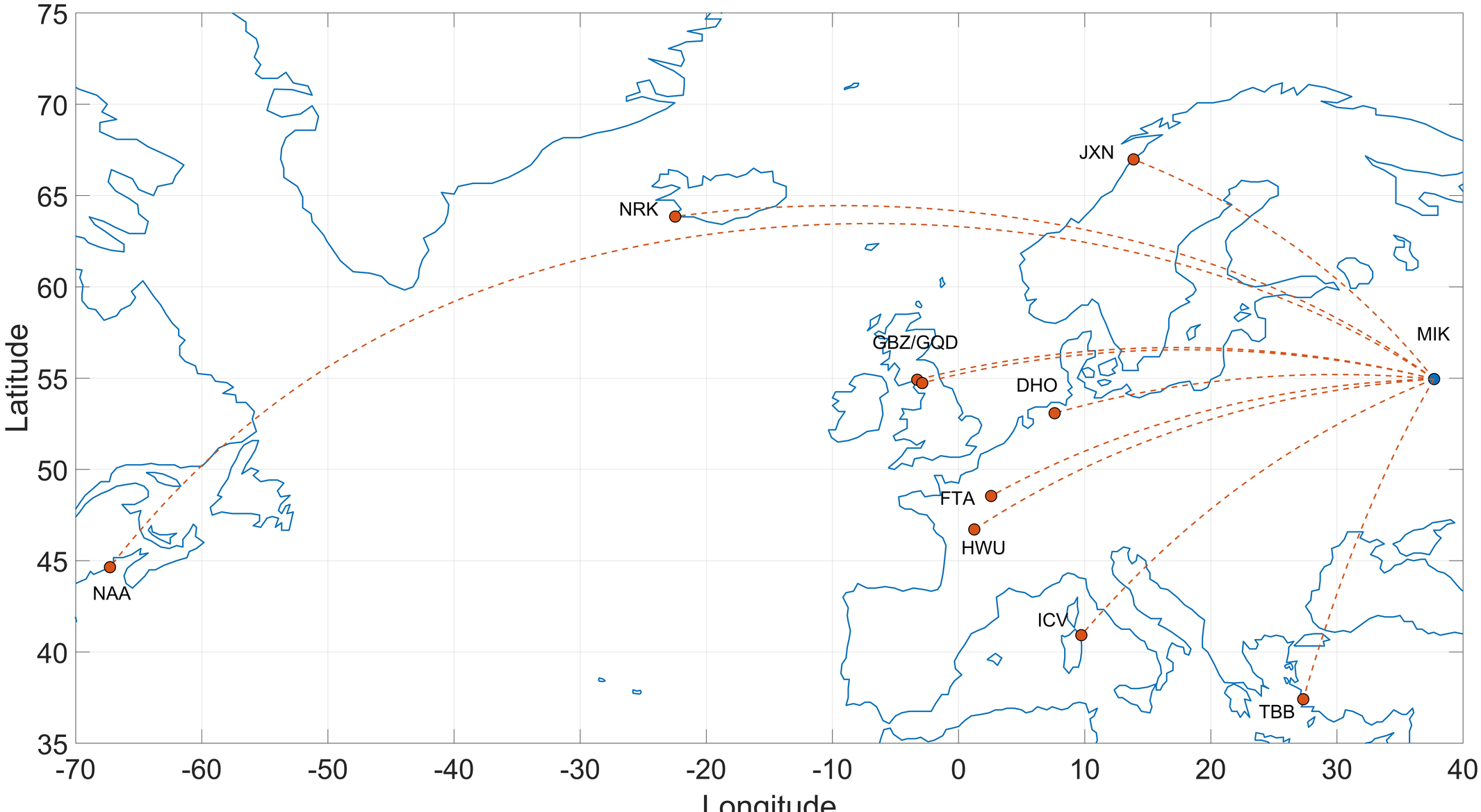
75
70
65
60
55
50
45
40
35
Latitude
-70
-60
-50
-40
-30
-20
-10
0
10
20
30
40
Longitude
JXN
NRK
MIK
GBZ/GQD
DHO
FTA
HWU
NAA
ICV
TBB

Figure 2.

X2.2 10.06.2014

a

X ray flux, W/m^2

10^{-4}

10^{-6}

10^{-8}

0.05-0.4 нм

0.1-0.8 нм

b

Amplitude, dB(pT)

7

6

5

4

3

GQD

GBZ

c

Phase, rad

1.5

1

0.5

0

GQD

GBZ

d

Ne, cm^{-3}

10^4

10^3

10^2

10^1

52 км

56 км

60 км

64 км

30 35 40 45 50 55 12:00 5 10 15 20 25 30

UT

Figure 3.

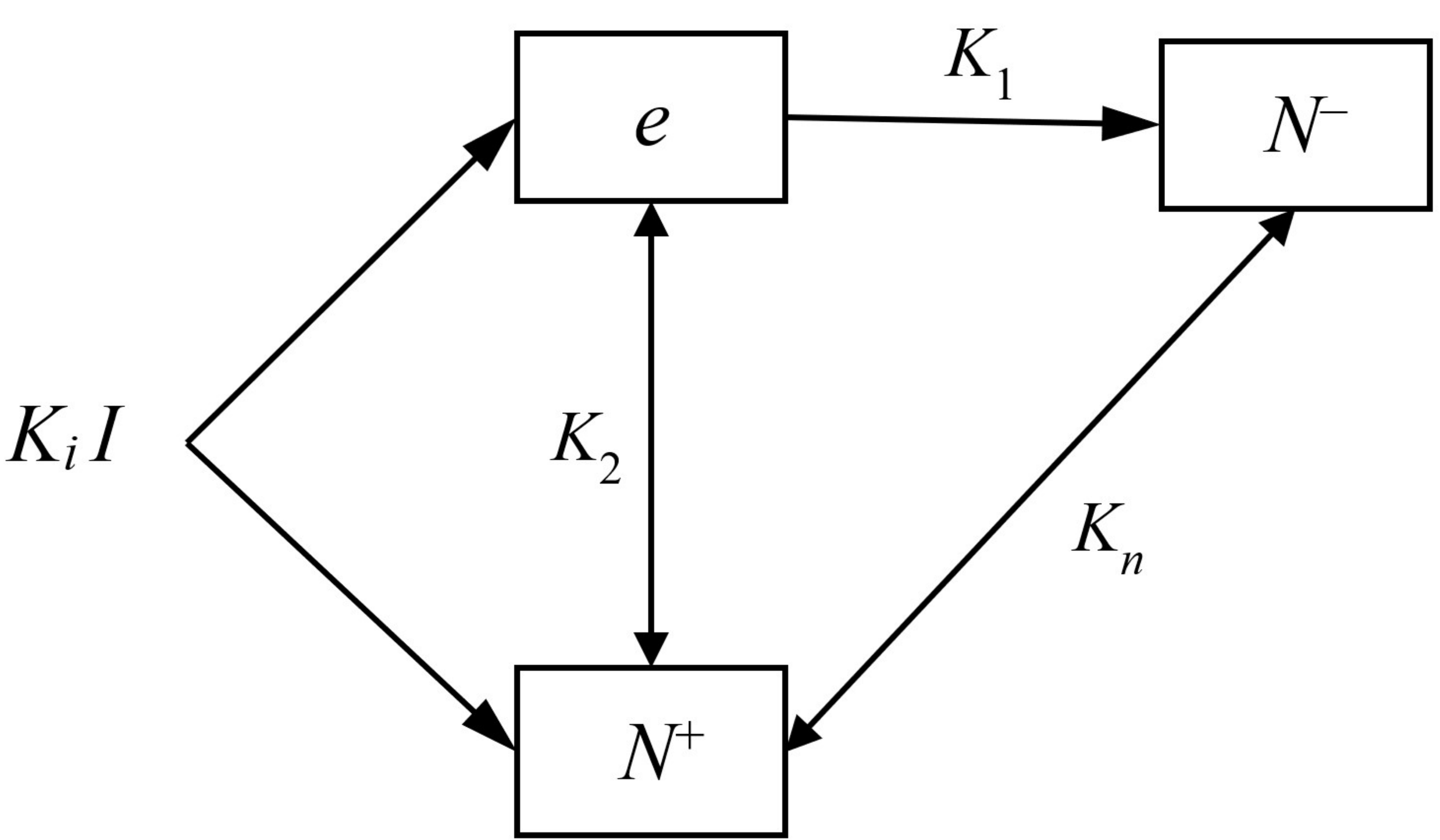
e
K_1
N^-
$K_i I$
K_2
K_n
N^+

Figure 4.

10.06.2014

F_2 (GOES 0.1-0.8 nm)
F_1 (GOES 0.05-0.4 nm)
0.01-0.3 nm
0.01-0.26 nm
0.01-0.22 nm

Flux, mW/m^2

10^{-1}
10^{-2}
10^{-3}
10^{-4}
10^{-5}
10^{-6}
10^{-7}
10^{-8}

30 35 40 45 50 55 12:00 5 10 15 20 25 30 35 40

UT

Figure 5.

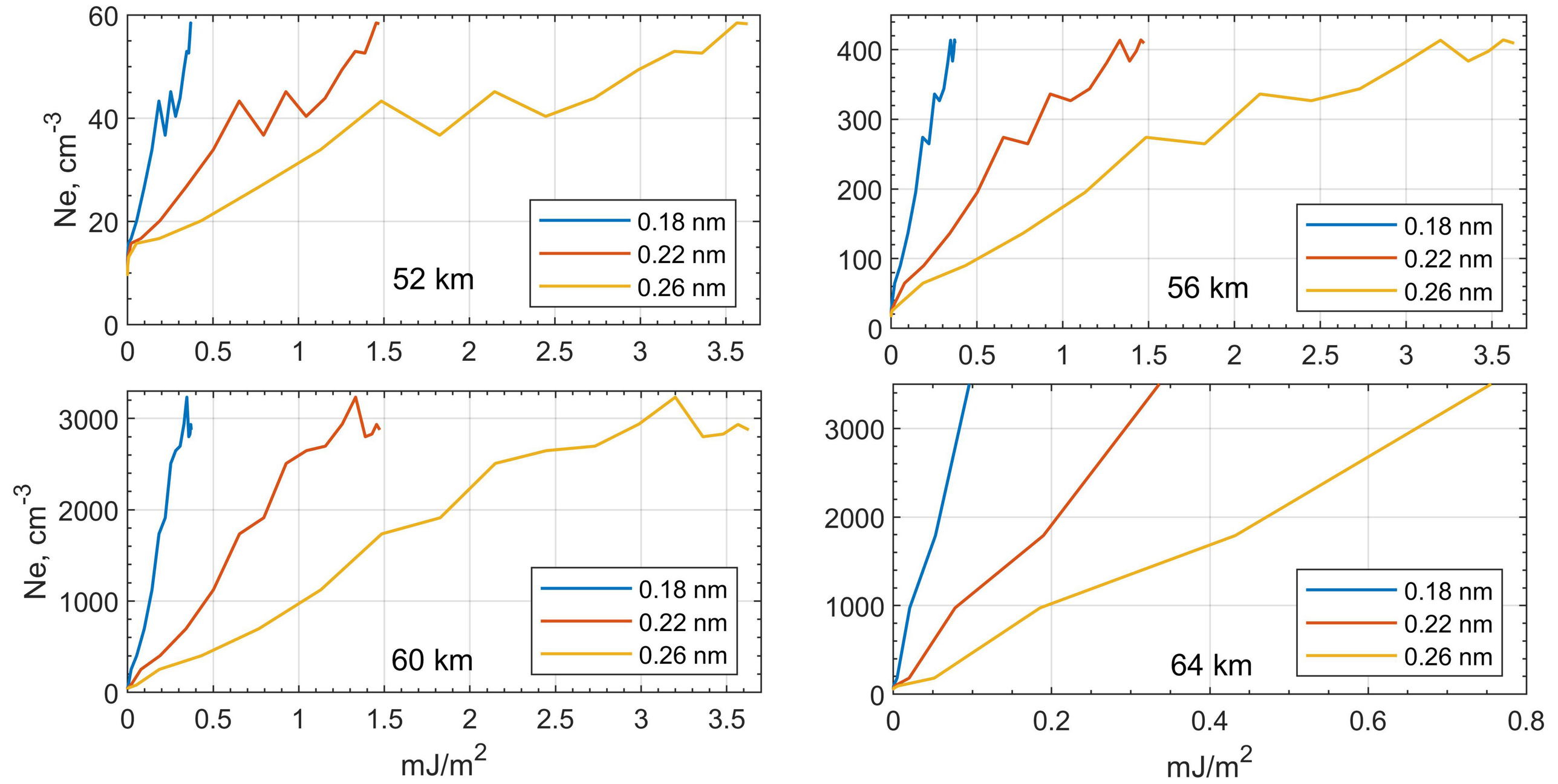
Ne, cm-3
52 km
0.18 nm
0.22 nm
0.26 nm
56 km
60 km
64 km
mJ/m2

Figure 6.

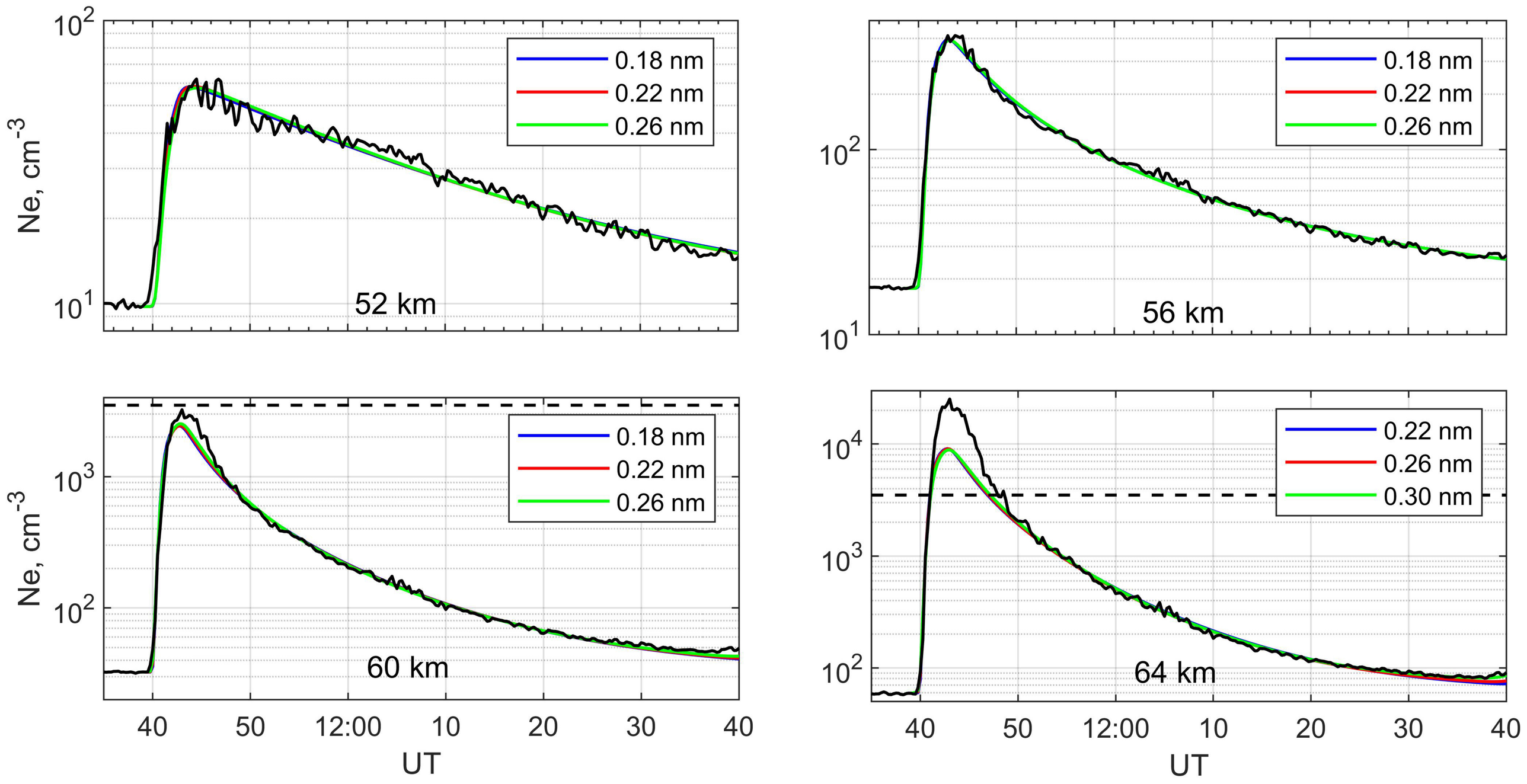
Ne, cm-3
0.18 nm
0.22 nm
0.26 nm
52 km
56 km
0.30 nm
60 km
64 km
40
50
12:00
10
20
30
40
UT

Figure 7.

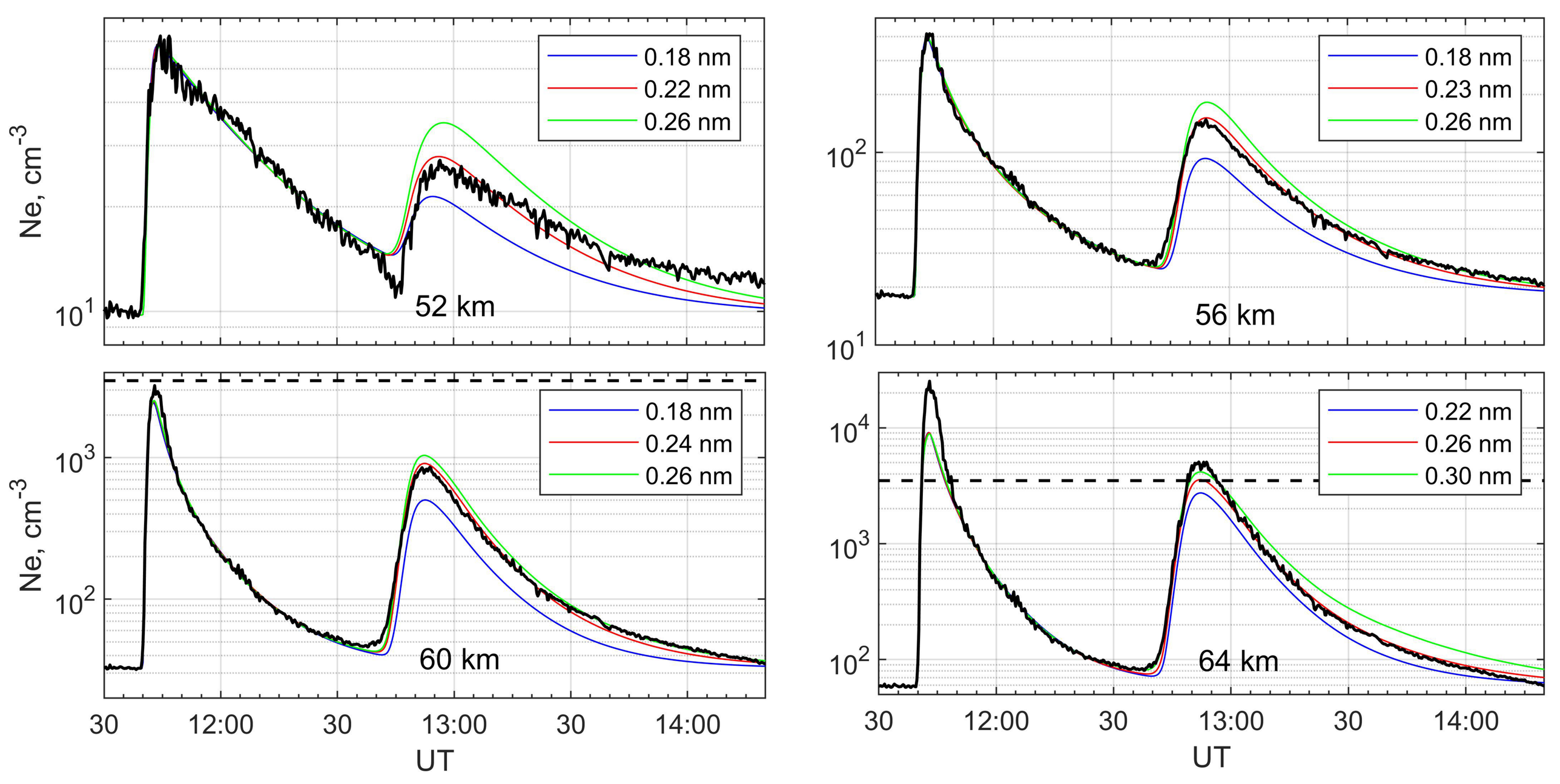
Ne, cm-3
0.18 nm
0.22 nm
0.26 nm
52 km
0.18 nm
0.23 nm
0.26 nm
56 km
0.18 nm
0.24 nm
0.26 nm
60 km
0.22 nm
0.26 nm
0.30 nm
64 km
30
12:00
30
13:00
30
14:00
UT

Figure 8.

10-06-2014 GQD C-class

a

b

pT

Radians

Experiment

Calculation

UT

11-06-2014 GQD M3

c

d

pT

Radians

UT